HAL
open science

A modal strategy devoted to the hidden state variables method with large interfaces

Pierre Ropars, Christophe Desceliers

To cite this version:

Pierre Ropars, Christophe Desceliers. A modal strategy devoted to the hidden state variables method with large interfaces. Computational Mechanics, 2015, 55 (5), pp.805-818. 10.1007/s00466-015-1148-z . hal-01140558

HAL Id: hal-01140558

https://hal.science/hal-01140558v1

Submitted on 8 Apr 2015

HAL is a multi-disciplinary open access archive for the deposit and dissemination of scientific research documents, whether they are published or not. The documents may come from teaching and research institutions in France or abroad, or from public or private research centers.

L'archive ouverte pluridisciplinaire **HAL**, est destinée au dépôt et à la diffusion de documents scientifiques de niveau recherche, publiés ou non, émanant des établissements d'enseignement et de recherche français ou étrangers, des laboratoires publics ou privés.

Computational Mechanics manuscript No.
(will be inserted by the editor)

A modal strategy devoted to the Hidden State Variables Method with large interfaces

Pierre Ropars · Christophe Desceliers

Received: date / Accepted: date

Abstract In many mechanical engineering applications, the interactions of a structure through its boundary is modelled by a dynamic boundary stiffness matrix. Nevertheless, it is well known that the solution of such computational model is very sensitive to the modelling uncertainties on the dynamic boundary stiffness matrix. In a recent work, the "hidden state variables method" is used to identify mass, stiffness and damping matrices associated with a given deterministic dynamic boundary stiffness matrix which can be constructed by using experimental measurements. Such an identification allows the construction of the probabilistic model of a random boundary stiffness matrix by substituting those identified mass, stiffness and damping matrices by random matrices. Nevertheless, the numerical cost of the "hidden state variables method" increases drastically with the dimension (number of degrees of freedom) of the interface. We then propose an enhanced approach which consists in a truncated spectral representation of the displacements on the boundary and with a partition of the frequency band of analysis. A collection of mass, stiffness and damping matrices is then identified for each sub-frequency band of analysis. A probabilistic model is constructed in substituting each of those matrices by random matrices. A numerical application is proposed.

P. Ropars
MSME Université Paris-Est Marne-la-Vallée; 5 Bd Descartes, 77454 Marne-la-Vallée cedex 2, France
E-mail: pierre.ropars@gmail.com

C. Desceliers
MSME Université Paris-Est Marne-la-Vallée; 5 Bd Descartes, 77454 Marne-la-Vallée cedex 2, France
E-mail: christophe.desceliers@univ-paris-est.fr

Keywords Finite elements method · Hidden state variables method · Random matrices · Random dynamic boundary stiffness matrix

1 Introduction

The uncertainties quantification of complex mechanical systems is a challenge for engineers and researchers. This paper deals with an inverse method in the Fourier space for the uncertainty quantification in a structural linear visco-elasto dynamics system in low frequency band.

The mechanical system under study is composed by Ω_2 which is coupled with Ω_1. It is assumed that a numerical model of Ω_2 can be constructed, while it is not the case for Ω_1. The coupling between Ω_1 and Ω_2 is performed on an interface Γ. For example, it is the case for the design of a building (Ω_2) whose foundations are coupled with an unknown soil (Ω_1). Nevertheless, it is usual to model the dynamical response of Ω_1 on the interface Γ by a boundary dynamical stiffness matrix which can be obtained by experimental measurements or by numerical computations.

The numerical derivation of the boundary stiffness matrix requires the resolution of a classical mixed boundary value problem. A large set of usual methods is therefore usable, among which the finite-elements method [1] is the most often used. When the domain Ω_1 becomes large, or unbounded, an artificial boundary has to be introduced. The truncation of the domain means that waves would reflect on the artificial boundary and pollute the solution in the domain Ω_2. Many techniques have been derived in the literature to prevent this problem. Some of them are reviewed in [2,3], or in special journal issues on absorbing boundary conditions [4–6].

These techniques can be gathered into three groups: global absorbing boundary conditions, local absorbing boundary conditions, and absorbing layer. Besides these finite-elements-based methods stands the boundary elements method [7]. Then, it appears quite natural for the computation of the boundary stiffness matrix, since the formulation is directly performed on the boundary and in case of an unbounded domain, the radiation conditions are directly taken into account. The scaled boundary elements method [8] is an alternative approach which does not require a fundamental solution, and only requires the meshing of the boundary and enforces naturally the radiation condition. The main requirement for this method is a particular type of radial symmetry of the domain. When the boundary stiffness matrices of Ω_1 and Ω_2 are computed separately, the mobility method allows the response of both Ω_1 and Ω_2 to be simulated when the two domains are coupled [9–11]. In an other point of view, the subsystem Ω_1 transposes on Γ a distant boundary condition. Several authors introduce a Dirichlet-to-Neumann map to describe, in the time domain, the external forces due to Ω_1 that are applied to Γ [2,12].

In addition, many methods have been proposed to reduce the number of degrees of freedom in a model [23]. We can cite the condensation techniques [24], or the truncated expansion techniques which are very popular. They are proposed in any computational problem which is concerned by large numerical cost. In the scope of soil-structure interaction problem, the boundary finite element method has received several significant advances [25,26]. Recent developments in the bridging scale method proposed an efficient response to a dynamical interface problem [27]. Also, in the time domain and in the scope of the Dirichlet-to-Neumann mapping, several authors have developed efficient methods [28–30]. This paper is concerned by a problem in the Fourier domain, and the method used hereinafter is based on an *ad-hoc* truncated expansion of eigenfunctions.

However, in the framework of the robust conception of Ω_2, it is necessary to quantify the uncertainties induced by the lack of knowledge on Ω_1. In this aim, a probabilistic approach is very efficient, and a probabilistic model of the uncertainties related to Ω_1 can be constructed by modelling the boundary dynamical stiffness matrix as a random matrix. In the last decade, a new probabilistic approach has been developed in linear visco-elasto dynamic in order to model the uncertainties related to the modelling of a mechanical system in constructing an *ad hoc* probabilistic model of the mass, damping and stiffness matrices [13,14]. In [15–17], such a probabilistic approach has been applied to construct the model of the random boundary dynamical stiffness matrix. It has been achieved with the identification of mass, damping and stiffness matrices corresponding to a dynamical stiffness matrix for which the Shur complement is equal to the boundary dynamical stiffness matrix of Ω_1.

The hidden state variables method [15,16,18,19] is an efficient method devoted to such an identification. Among all the degrees of freedom associated with the identified mass, damping and stiffness matrices, those that do not belong to interface Γ are called hidden variables. It should be noted that they are not physical degrees of freedom, but "meta" degrees of freedom which give an equivalent description of the dynamical response of Ω_1 on the interface. It is assumed that (1) the unknown complete dynamical model of Ω_1 is a second-order differential equation; (2) the boundary dynamic stiffness matrix is symmetric and continuous on the frequency band of analysis B_{f}; (3) the mass, damping and stiffness matrices to be identified are real, symmetric and positive-definite. These assumptions have physical interpretation, and assure the preservation of principles of reciprocity [20] and causality [21].

Despite numerous advantages, some numerical difficulties occur with an extensive use of the hidden state variables method: the stability and the numerical cost. In [22] and [19], the stability issue has been addressed. The numerical cost increases with the dimension of the problem (number of degrees of freedom of the interface). Indeed, computational time increases drastically when the dimension is greater than 10, even with a reasonable frequency band of analysis. The extension of the hidden state variables method in high dimension remains a challenge. This would allow a realistic mechanical system with a high dimension to be studied. Consequently, we propose hereinafter a formulation that allows such an extension without modification of the numerical algorithms used in the hidden state variable method in order to carry out the identification. This is achieved by introducing a reduced representation of the displacements field on interface Γ for sub-frequency bands of analysis included in B_{f}.

In the second section of the paper, the boundary dynamic stiffness matrix and the dynamic equation of Ω_2 are presented. The following section deals with the reduction of the problem and its decomposition on several sub-frequency bands of analysis. Then, in the fourth section, the hidden state variables method is briefly presented. Then, a probabilistic model for the random boundary dynamic stiffness matrix is formulated for each sub-frequency bands of analysis. It should be noted that the proposed approach yields a set statistically independent random mass, damping and stiffness matrices for each sub-frequency bands of analysis. Some nu-

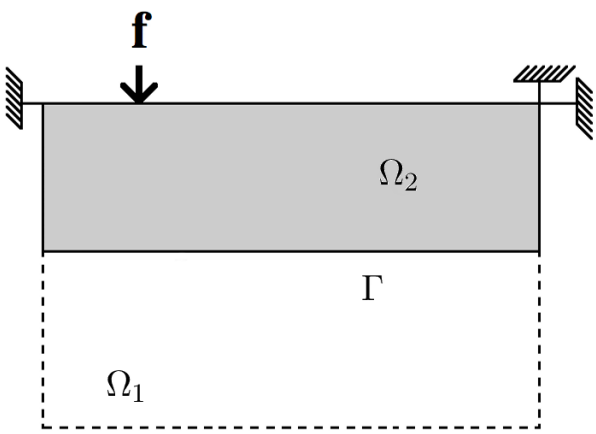

Fig. 1 Geometry of domain Ω.

merical applications are given in section 5.3, 5.4, 5.5, 5.6 and 6.2 in order to study the efficiency of the proposed approach.

2 Boundary dynamic stiffness matrix and dynamic equation of Ω_2

We consider a structure modelled in Fourier space by a visco-elastic medium and that is occupying a bounded domain denoted by Ω. Domain Ω is made up of two distinct sub-domains denoted by Ω_1 and Ω_2. Let Γ be the interface between Ω_1 and Ω_2 (see Fig. 1). A finite-element interpolation basis is used to calculate a numerical approximation of the displacement field $\mathbf{x} \mapsto \mathbf{u}(\mathbf{x}, \omega)$ in Ω_2 in which $\mathbf{x}$ is the vector of coordinates of any generic point in Ω_2 and ω is the angular frequency. For all ω in the frequency band of analysis B_{f}, let $\mathbf{u}_2(\omega) \in \mathbb{R}^{n_2}$ be the vector of all the degrees of freedom of the finite-element interpolation and let the mass, damping and stiffness real $(n_2 \times n_2)$ matrices be denoted by $[M_2]$, $[D_2]$ and $[K_2]$. For all frequency ω in B_{f}, the dynamic stiffness matrix $[A_2(\omega)]$ of domain Ω_2 is then written as

$$[A_2(\omega)] = -\omega^2 [M_2] + \jmath\, \omega [D_2] + [K_2] \ . \tag{1}$$

The coupling between the two visco-elastic media occupying Ω_1 and Ω_2 is taken into account in constructing the boundary dynamic stiffness $[A_\Gamma(\omega)]$ associated with the displacements on interface Γ and which is a symmetric $(n_\Gamma \times n_\Gamma)$ matrix where n_Γ is the number of degree of freedom on Γ for the finite element model of Ω_2. Let us assume that the numbering of the degrees of freedom is such that $\mathbf{u}_2(\omega)$ is written as

$$\mathbf{u}_2(\omega) = \begin{pmatrix} \mathbf{u}_{\Omega_2}(\omega) \\ \mathbf{u}_\Gamma(\omega) \end{pmatrix} \ , \tag{2}$$

where $\mathbf{u}_{\Omega_2}(\omega)$ is the vector of the $n_2 - n_\Gamma$ degrees of freedom related to nodes of the finite-element mesh in Ω_2 and $\mathbf{u}_\Gamma(\omega)$ is the vector of the n_Γ degrees of freedom related to the nodes on interface Γ. We then have, for all ω in B_{f},

$$([A_2(\omega)] + [A(\omega)])\, \mathbf{u}_2(\omega) = \mathbf{f}(\omega) \ , \tag{3}$$

where $\mathbf{f}(\omega) \in \mathbb{R}^{n_2}$ is the finite-element vector of the external forces applied on structure and in which the block diagonal matrix $[A(\omega)]$ is written as

$$[A(\omega)] = \begin{pmatrix} [0_2] & \\ & [A_\Gamma(\omega)] \end{pmatrix} \ , \tag{4}$$

where the $(n_2 - n_\Gamma \times n_2 - n_\Gamma)$ real matrix $[0_2]$ is the null matrix.

3 Reduced representation of the displacement at the interface

3.1 Spectral functional basis adapted for domain Ω_2 with a coupled interface Γ

The main idea of the proposed approach is to reduce the number of degrees of freedom representing the displacements on interface Γ. Such a reduction is carried out in rewriting the dynamical system in using an *ad hoc* functional basis. A very efficient functional basis that is widely used in the literature consists in the eigenfunctions associated with the generalized eigenvalue problem for the whole domain Ω. In our situation, the numerical model of sub-domain Ω_1 is assumed to be not given. Another functional basis can be made up of the eigenfunctions associated with the generalized eigenvalue problem of sub-domain Ω_2 with fixed interface Γ or with free interface Γ. Nevertheless, the additional mass, damping and stiffness due to the coupling with sub-domain Ω_1 are not taking into account. Consequently, a high number of eigenfunction should be used in order to represent accurately the displacement field on the interface. It is the reason why we introduce the following generalized eigenvalue problem: find eigenvectors $\boldsymbol{\phi}_\alpha \in \mathbb{R}^{n_2}$ and eigenvalues λ_α such as

$$[\mathbb{K}_2]\boldsymbol{\phi}_\alpha = \lambda_\alpha [\mathbb{M}_2]\boldsymbol{\phi}_\alpha \ , \tag{5}$$

in which

$$[\mathbb{K}_2] = [K_2] + \mathcal{R}\{[A(0)]\} \ , \tag{6}$$

and

$$[\mathbb{M}_2] = [M_2] + \frac{1}{c} \int_{B_{\mathrm{f}}} \mathcal{R}\{[A(\omega)] - [A(0)]\}\, d\omega \ , \tag{7}$$

where $\mathcal{R}\{[a]\}$ means the real part of any complex matrix $[a]$ and $c = -\int_{B_\mathrm{f}} \omega^2 \, d\omega$. The additional terms in the right side of Eqs (6) and (7) corresponds to additional mass and stiffness due to the coupling of interface Γ with sub-domain Ω_1. Similarly, we introduce a damping matrix $\mathbb{D}_2$ defined as

$$[\mathbb{D}_2(\omega)] = [D_2] + \mathcal{I}\{[A(\omega)]\} \ , \tag{8}$$

where $\mathcal{I}\{[a]\}$ means the imaginary part of any complex matrix $[a]$. The additional term in the right side of Eq (8) corresponds to an additional damping due the coupling of interface Γ with subdomain Ω_1. It is assumed that matrices $[\mathbb{M}_2]$ and $[\mathbb{K}_2]$ are definite-positive. Consequently, this generalized eigenvalue problem yields an increasing sequence of eigenvalues $0 < \lambda_1 \leq \lambda_2 \leq \ldots \leq \lambda_{n_2}$, associated with the eigenvectors $\boldsymbol{\phi}^1$, ..., $\boldsymbol{\phi}^{n_2}$ in $\mathbb{R}^{n_2}$. For any given $\alpha = 1, \ldots, n_2$, the eigenfrequency ω_α (in rad/s) is defined as $\omega_\alpha = \lambda_\alpha^{1/2}$. The numbering of the degrees of freedom is such that, for any $\alpha = 1, \ldots, n_2$ eigenvector $\boldsymbol{\phi}^\alpha$ is written as

$$\boldsymbol{\phi}^\alpha = \begin{pmatrix} \boldsymbol{\phi}^\alpha_{\Omega_2} \\ \boldsymbol{\phi}^\alpha_\Gamma \end{pmatrix} \ , \tag{9}$$

where $\boldsymbol{\phi}^\alpha_{\Omega_2}$ is the vector of the $n_2 - n_\Gamma$ degrees of freedom related to nodes in Ω_2 and $\boldsymbol{\phi}^\alpha_\Gamma$ is the vector of the n_Γ degrees of freedom related to the nodes on interface Γ. The set of vectors $\boldsymbol{\phi}^1_\Gamma, \ldots, \boldsymbol{\phi}^{n_2}_\Gamma$ can be used in order to construct a spectral representation of vector $\mathbf{u}_\Gamma$ but it should be noted that this set of vectors are linearly dependent and consequently, they do not define an *ad hoc* functional basis.

3.2 Decomposition of the frequency band of analysis B_f

For using the hidden state variables method with vectors $\boldsymbol{\phi}^1_\Gamma, \ldots, \boldsymbol{\phi}^{n_2}_\Gamma$ as spectral functional basis of the displacements on interface Γ, we introduce a decomposition of the frequency band of analysis B_f into n_f frequency bands $B_1, \ldots, B_{n_\mathrm{f}}$ which are not necessarily disjoints and such that $B_\mathrm{f} = \cup_{k=1}^{n_\mathrm{f}} B_k$. Let the m_k eigenfrequencies $\omega_{k,1} \leq \ldots \leq \omega_{k,m_k}$ be all the eigenfrequencies belonging to B_k. Then, for $k = 1, \ldots, n_\mathrm{f}$, the construction of the k-th frequency band B_k is such that

$$[\omega_{k,1} - \frac{H_{k,1}}{2}, \ \omega_{k,m_k} + \frac{H_{k,m_k}}{2}] \subset B_k \ , \tag{10}$$

where $H_\alpha = \pi \xi_\alpha \omega_\alpha \sqrt{1 - \xi_\alpha^2}$ with $\xi_\alpha = D_\alpha / 2\sqrt{M_\alpha \, K_\alpha}$ and $M_\alpha = (\boldsymbol{\phi}^\alpha)^T [\mathbb{M}_2] \, \boldsymbol{\phi}^\alpha$, $D_\alpha = (\boldsymbol{\phi}^\alpha)^T [\mathbb{D}_2(\omega_\alpha)] \, \boldsymbol{\phi}^\alpha$ and $K_\alpha = (\boldsymbol{\phi}^\alpha)^T [\mathbb{K}_2] \, \boldsymbol{\phi}^\alpha$. Two special cases can be considered. The first special case is obtained with $n_\mathrm{f} = 1$ ($k = 1$ and $m_k = n_2$) and the second special case is obtained with $m_k = 1$ ($n_\mathrm{f} = n_2$ and $m_k = 1$ for all $1 \leq k \leq n_2$). Beside these two cases, any other combination is also possible. Note that, when m_k is constant for all B_k, the number of frequency bands n_f is fixed. This configuration is used hereinafter in Sections 5 and 6.2. In order to ensure that all frequencies of B_f are contained at least in one B_k, each frequency band B_k can be taken as :

$$B_k = [(\omega_{k-1,m_{k-1}} + \frac{H_{k-1,m_{k-1}}}{2} + \omega_{k,1} - \frac{H_{k,1}}{2})/2, \\ (\omega_{k,m_k} + \frac{H_{k,m_k}}{2} + \omega_{k+1,1} - \frac{H_{k+1,1}}{2})/2] \ . \tag{11}$$

3.3 Reduced interface displacement model in each frequency band B_k

We introduce the $(n_\Gamma \times m_k)$ interface modal matrix $[\phi_{\Gamma,B_k}]$ which is such that its ℓ-th column is vector $\boldsymbol{\phi}^{k,\ell}_\Gamma$ (see Eq. 9) associated with $\omega_{k,\ell}$ which is the ℓ-th eigenfrequency in B_k. An orthogonal basis is deduced by the singular value decomposition of matrix $[\phi_{\Gamma,B_k}]$ written as

$$[\phi_{\Gamma,B_k}] = [U_{\Gamma,B_k}][\Sigma_{\Gamma,B_k}][V_{\Gamma,B_k}]^T \ , \tag{12}$$

where $[U_{\Gamma,B_k}]$ is an unitary $(n_\Gamma \times n_\Gamma)$ matrix, $[\Sigma_{\Gamma,B_k}]$ is a $(n_\Gamma \times m_k)$ matrix whose only elements on its diagonal are non zero and where $[V_{\Gamma,B_k}]$ is an unitary $(m_k \times m_k)$ matrix. It is assumed that the singular values of $[\phi_{\Gamma,B_k}]$ are listed in descending order on the diagonal of $[\Sigma_{\Gamma,B_k}]$. Consequently, we have the following block decomposition of $[U_{\Gamma,B_k}]$,

$$[U_{\Gamma,B_k}] = \left([U^+_{\Gamma,B_k}] \ [U^0_{\Gamma,B_k}] \right) \ , \tag{13}$$

where the columns of $[U^+_{\Gamma,B_k}]$ are all the vectors associated with all the non-zero singular values of $[\phi_{\Gamma,B_k}]$. Let $m^+_{B_k}$ be the number of non-zero singular values of $[\phi_{\Gamma,B_k}]$. Note that, in general, $m^+_{B_k} = \min(n_\Gamma, m_k)$, but in the following $m^+_{B_k} = m_k$. For any given frequency ω in B_k, we introduce the $m^+_{B_k}$-order approximation $\mathbf{u}_{\Gamma,B_k}(\omega)$ of vector $\mathbf{u}_\Gamma(\omega)$ defined as

$$\mathbf{u}_{\Gamma,B_k}(\omega) = [U^+_{\Gamma,B_k}] \, \mathbf{q}_{B_k}(\omega) \ , \tag{14}$$

where $\mathbf{q}_{B_k}(\omega)$ is the vector of the $m^+_{B_k}$ generalized interface displacements on interface Γ for the frequency band B_k. For any given ω in B_k, we then have the following approximation $\mathbf{u}_{2,B_k}(\omega)$ of vector $\mathbf{u}_2(\omega)$,

$$\mathbf{u}_{2,B_k}(\omega) = [P_{B_k}] \, \mathbb{u}_{2,B_k}(\omega) \ , \tag{15}$$

in which the block diagonal matrix $[P_{B_k}]$ and the reduced representation $\mathbb{u}_{2,B_k}(\omega)$ of $\mathbf{u}_{2,B_k}$ are written as

$$[P_{B_k}] = \begin{pmatrix} [I_2] & \\ & [U^+_{\Gamma,B_k}] \end{pmatrix} \quad \text{and} \quad \mathbb{u}_{2,B_k}(\omega) = \begin{pmatrix} \mathbf{u}_{\Omega_2}(\omega) \\ \boldsymbol{q}_{B_k}(\omega) \end{pmatrix} \ ,$$

(16)

where $[I_2]$ is the $(n_2 - n_\Gamma \times n_2 - n_\Gamma)$ identity matrix. Multiplying each side of Eq. (3) by $[P_{B_k}]^T$ and in using Eq. (16), we then obtain

$$([A_{2,B_k}(\omega)] + [A_{B_k}(\omega)])\, \mathbb{u}_{2,B_k}(\omega) = \mathbb{f}_{B_k}(\omega) \ , \tag{17}$$

in which $\mathbb{f}_{B_k}(\omega) = [P_{B_k}]^T \mathbf{f}(\omega)$ and where the square matrices of dimension $(n_2 - n_\Gamma + m^+_{B_k})$ $[A_{2,B_k}(\omega)]$ and $[A_{B_k}(\omega)]$ are defined as

$$[A_{2,B_k}(\omega)] = [P_{B_k}]^T \, [A_2(\omega)] \, [P_{B_k}] \ , \tag{18}$$

and

$$[A_{B_k}(\omega)] = [P_{B_k}]^T \, [A(\omega)] \, [P_{B_k}] = \begin{pmatrix} [0_2] & \\ & [A_{\Gamma,B_k}(\omega)] \end{pmatrix} \ , \tag{19}$$

in which the symmetric $(m^+_{B_k} \times m^+_{B_k})$ matrix $[A_{\Gamma,B_k}(\omega)] = [U^+_{\Gamma,B_k}]^T \, [A_\Gamma(\omega)] \, [U^+_{\Gamma,B_k}]$ is the reduced boundary dynamic boundary stiffness matrix associated with the displacements on interface Γ.

4 The hidden state variable method

Hereinafter, a short overview of the hidden state variables method is presented. For more details, the reader can refer to [15,16].

4.1 Algebraic representation of the boundary stiffness matrix $[A_\Gamma(\omega)]$

For a large range of engineering applications, boundary stiffness matrix $[A_\Gamma(\omega)]$ (see Eqs. (3) and (4)) is obtained in using experimental measurements in dynamics. It is the case when a numerical model of Ω_1 is tricky to be constructed. The hidden states variables method can be used in order to identify a symmetric positive definite $(n_1 \times n_1)$ matrix $[M_1]$ and two symmetric positive $(n_1 \times n_1)$ matrices $[D_1]$ and $[K_1]$ such that

$$[A_\Gamma(\omega)] = [A_{1\Gamma}(\omega)] - [A_{1c}(\omega)] \, [A_{1h}(\omega)]^{-1} [A_{1c}(\omega)]^T \ , \tag{20}$$

in which the symmetric $(n_\Gamma \times n_\Gamma)$ matrix $[A_{1\Gamma}(\omega)]$, the $(n_1 - n_\Gamma \times n_\Gamma)$ matrix $[A_{1c}(\omega)]$ and the symmetric $(n_1 - n_\Gamma \times n_1 - n_\Gamma)$ matrix $[A_{1h}(\omega)]$ are obtained from the block decomposition of the dynamic stiffness matrix $[A_1(\omega)] = -\omega^2 [M_1] + \jmath\, \omega [D_1] + [K_1]$ written as

$$[A_1(\omega)] = \begin{pmatrix} [A_{1h}(\omega)] & [A_{1c}(\omega)] \\ [A_{1c}(\omega)]^T & [A_{1\Gamma}(\omega)] \end{pmatrix} \ , \tag{21}$$

where the numbering of the degree of freedom are such that the n_Γ last rows and the n_Γ last columns of $[A_1(\omega)]$ are related to the n_Γ degrees of freedom of nodes on Γ.

4.2 Step 1 : Interpolation of the given boundary dynamic stiffness matrix

The first step of the method consists in constructing an interpolation of $\omega \mapsto [A_\Gamma(\omega)]$. Boundary dynamic stiffness matrix is rewritten as $[A_\Gamma(\omega)] = [N^{\text{opt}}(\omega)]/q^{\text{opt}}(\omega)$ in which $[N^{\text{opt}}]$ belongs to $\mathcal{S}(n_\Gamma, d_N)$ and q^{opt} belongs to $\mathcal{S}(1, d_q)$ where $\mathcal{S}(n, d)$ means the set of all polynomial functions of degree d with values in the set of all the symmetric $(n \times n)$ matrices. The two polynomial functions $[N^{\text{opt}}]$ and q^{opt} are then defined as the optimal functions solving an optimization problem. We then have, in [15],

$$([N^{\text{opt}}], q^{\text{opt}}) = \arg \min_{\substack{q \in \mathcal{S}(1,d_q) \\ [N] \in \mathcal{S}(n_\Gamma, d_N)}} \varepsilon([N], q) \ , \tag{22}$$

with $d_N = d_q + 2$ and where

$$\varepsilon([N], q) = \int_{B_{\text{f}}} c(\omega)^2 \left\| \frac{[N(\omega)]}{q(\omega)} - [A_\Gamma(\omega)] \right\|^2_{\text{F}} d\omega \ , \tag{23}$$

and $\omega \mapsto c(\omega)$ is a regularizing function [31] and $\|.\|_{\text{F}}$ is the Frobenius norm of symmetric matrices. The algorithm presented in [15] to solve Eq. (22) requires to perform the numerical orthogonalization of $m_h = (n_\Gamma^2 + n_\Gamma)(d_q + 3)/2 + (d_q + 1)$ vectors belonging to $\mathbb{C}^d$ with $d = (n_\Gamma^2 + n_\Gamma)/2 + 1$. This numerical orthogonalization is carried out in using a Gram-Schmidt algorithm.

4.3 Step 2: Identification of a matrix model for the hidden variables

The last step of the hidden state variables method consists in identifying a set of matrices $[M_1^{\text{opt}}]$, $[D_1^{\text{opt}}]$ and $[K_1^{\text{opt}}]$ such that

$$\frac{[N^{\text{opt}}(\omega)]}{q^{\text{opt}}(\omega)} = [A^{\text{opt}}_{1\Gamma}(\omega)] - [A^{\text{opt}}_{1c}(\omega)] \, [A^{\text{opt}}_{1h}(\omega)]^{-1} [A^{\text{opt}}_{1c}(\omega)]^T \ , \tag{24}$$

where the symmetric $(n_\Gamma \times n_\Gamma)$ matrix $[A^{\text{opt}}_{1\Gamma}(\omega)]$, the complex $(n_1 - n_\Gamma \times n_\Gamma)$ matrix $[A^{\text{opt}}_{1c}(\omega)]$ and the symmetric $(n_1 - n_\Gamma \times n_1 - n_\Gamma)$ matrix $[A^{\text{opt}}_{1h}(\omega)]$ are obtained from the block decomposition of the dynamic stiffness matrix

$$[A^{\text{opt}}_1(\omega)] = -\omega^2 [M^{\text{opt}}_1] + \jmath\, \omega [D^{\text{opt}}_1] + [K^{\text{opt}}_1] \ , \tag{25}$$

which is then written as

$$[A_1^{\rm opt}(\omega)] = \begin{pmatrix} [A_{1h}^{\rm opt}(\omega)] & [A_{1c}^{\rm opt}(\omega)] \\ [A_{1c}^{\rm opt}(\omega)]^T & [A_{1\Gamma}^{\rm opt}(\omega)] \end{pmatrix} \ . \tag{26}$$

An algorithm presented in [15] seeks for a block diagonal matrix $[M_1^{\rm opt}]$ written as

$$[M_1^{\rm opt}] = \begin{pmatrix} [I_{n_{\rm h}}] & \\ & [M_{1\Gamma}^{\rm opt}] \end{pmatrix} \ , \tag{27}$$

where $[I_{n_{\rm h}}]$ is the $(n_{\rm h} \times n_{\rm h})$ identity matrix with $n_{\rm h} = d_q/2$. It should be noticed that Eq. (27) is justified in [15]. Since that for any given frequency band of analysis $B_{\rm f}$, any given polynomial degree d_q and for any given boundary dynamic stiffness matrix $[A_\Gamma]$, it is possible to find a set of three matrices $[M_1^{\rm opt}]$, $[D_1^{\rm opt}]$ and $[K_1^{\rm opt}]$ which is constructed in solving (see [22,19,32]), then, it means that $([M_1^{\rm opt}], [D_1^{\rm opt}], [K_1^{\rm opt}])$ is the output value of a mapping $\mathcal{C}$,

$$([M_1^{\rm opt}], [D_1^{\rm opt}], [K_1^{\rm opt}]) = \mathcal{C}(B_{\rm f}; d_q, [A_\Gamma])) \ . \tag{28}$$

Hence, giving the identified matrices $[M_1^{\rm opt}]$, $[D_1^{\rm opt}]$ and $[K_1^{\rm opt}]$, then the matrix $[A_\Gamma^{\rm opt}(\omega)]$ which is defined as $[A_\Gamma^{\rm opt}(\omega)] = [A_{1\Gamma}^{\rm opt}(\omega)] - [A_{1c}^{\rm opt}(\omega)]\,[A_{1h}^{\rm opt}(\omega)]^{-1}[A_{1c}^{\rm opt}(\omega)]^T$ (see Eqs (25) and (26)), can be used as an approximation of the boundary dynamic boundary stiffness matrix $[A_\Gamma(\omega)]$.

4.4 Remark on the numerical cost of the method

The computational cost of the hidden state variables method is mostly due to the numerical orthogonalization of $m_h = (n_\Gamma^2 + n_\Gamma)(d_q+3)/2 + (d_q+1)$ vectors belonging to $\mathbb{C}^d$ with $d = (n_\Gamma^2 + n_\Gamma)/2 + 1$ (see section 4.2). Consequently, the greater n_Γ is and the more expensive is the hidden state variables method. For example, the Table 1 shows the computational time for performing the step 1 with respect to the number of degree of freedom n_Γ on the interface Γ for a very small problem (only 60 points in the frequency band and with $d_q = 2$). Such a computational cost for performing step 1 increases exponentially and consequently such a method is extremely expensive for dynamical systems with a high number of freedom on the interface Γ.

In this paper, the proposed approach is to decrease such numeral cost in using the *ad hoc* functional basis presented in Section 3.

Table 1 Computational cost of step 1 against the number of degree of freedom n_Γ on interface Γ.

n_Γ	Computational times (s)
2	6,5538
4	12,4342
6	55,3256
8	183,9891
10	510,1938
14	3214,5
18	14132,0
22	50331,0
28	360820,0

4.5 Hidden state variables method applied on the boundary dynamic stiffness matrices of Ω_1 for each frequency band B_k

For each frequency band B_k, the hidden state variables method is applied, with a polynomial degree d_{q,B_k}, yielding the construction of matrices $[M_{1,B_k}^{\rm opt}]$, $[D_{1,B_k}^{\rm opt}]$ and $[K_{1,B_k}^{\rm opt}]$ defined as

$$([M_{1,B_k}^{\rm opt}], [D_{1,B_k}^{\rm opt}], [K_{1,B_k}^{\rm opt}]) = \mathcal{C}(B_k; d_{q,B_k}, [A_{\Gamma,B_k}])) \ . \tag{29}$$

For each frequency band B_k, a stiffness matrix $[A_{1,B_k}^{\rm opt}(\omega)]$ is introduced as follows

$$[A_{1,B_k}^{\rm opt}(\omega)] = \\ -\omega^2[M_{1,B_k}^{\rm opt}] + \jmath\,\omega[D_{1,B_k}^{\rm opt}] + [K_{1,B_k}^{\rm opt}] \ . \tag{30}$$

The boundary stiffness matrix $[A_{\Gamma,B_k}^{\rm opt}(\omega)]$ is then defined as

$$[A_{\Gamma,B_k}^{\rm opt}(\omega)] = \\ [A_{1\Gamma,B_k}^{\rm opt}(\omega)] - [A_{1c,B_k}^{\rm opt}(\omega)]\,[A_{1h,B_k}^{\rm opt}(\omega)]^{-1}[A_{1c,B_k}^{\rm opt}(\omega)]^T, \tag{31}$$

where matrices $[A_{1\Gamma,B_k}^{\rm opt}(\omega)]$, $[A_{1c,B_k}^{\rm opt}(\omega)]$, $[A_{1h,B_k}^{\rm opt}(\omega)]$ and $[A_{1c,B_k}^{\rm opt}(\omega)]$ are extracted from the block decomposition of matrix $[A_{1,B_k}^{\rm opt}(\omega)]$. We then have

$$[A_{1,B_k}^{\rm opt}(\omega)] = \begin{pmatrix} [A_{1h,B_k}^{\rm opt}(\omega)] & [A_{1c,B_k}^{\rm opt}(\omega)] \\ [A_{1c,B_k}^{\rm opt}(\omega)]^T & [A_{1\Gamma,B_k}^{\rm opt}(\omega)] \end{pmatrix} \ . \tag{32}$$

Hence, for each frequency band B_k, the reduced representation $\mathbb{u}_{2,B_k}(\omega)$ of $\mathbf{u}_{2,B_k}(\omega)$ in Eq. (15) is constructed by solving Eq. (17) and in substituting the boundary dynamic boundary stiffness matrix $[A_{\Gamma,B_k}(\omega)]$ in Eq.(19) by matrix $[A_{\Gamma,B_k}^{\rm opt}(\omega)]$.

5 Examples of mass, dumping and stiffness matrices identification

In this section we propose four examples. In the two first, the mass, damping and stiffness matrices of domain Ω_1 are identified in using the hidden state variables method that is briefly recalled in Section 4 (initial method), and in using the hidden state variables method applied on the boundary dynamic stiffness matrices of Ω_1 for each frequency band B_k as it is presented in Section 4.5 (modified method). In third and fourth example, only results of modified method are presented because of the lack of accuracy and because of the computational cost of the initial method.

5.1 Description of the examples

For the following examples, domain Ω (see Section 2) is composed of two sub-domains Ω_1 and Ω_2 (see Fig. 1) that are assumed to be occupied by two homogeneous isotropic viscoelastic media in 2D plane strains. Let $E_1 = 26 \times 10^6$ Pa, $\nu_1 = 0.3$, $\rho_1 = 1600$ kg/m^3 be the Young modulus, the Poisson coefficient and the mass density in Ω_1 and let $E_2 = 26 \times 10^9$ Pa, $\nu_2 = 0.257$ and $\rho_2 = 2400$ kg/m^3 be the Young modulus, the Poisson coefficient and the mass density in Ω_2. Two points of Ω_2 (see Fig. 1) are blocked and the density of frequencies is 20 points per Hertz.

5.2 Boundary frequency response function

In order to compare the initial method and the modified method that we propose, the boundary dynamic stiffness matrix has to be written in the same functional basis. Nevertheless, it is not possible to rewrite matrices $[A^{\text{opt}}_{\Gamma,B_k}(\omega)]$ on the same basis as $[A^{\text{opt}}_{\Gamma}(\omega)]$ because we used a projection on interface displacement. It is the reason why we construct the boundary dynamic response function for each method.

As explained in Section 2, it is assumed that the numbering of the degrees of freedom is such that $\mathbf{u}_2(\omega)$ is written as

$$\mathbf{u}_2(\omega) = \begin{pmatrix} \mathbf{u}_{\Omega_2}(\omega) \\ \mathbf{u}_{\Gamma}(\omega) \end{pmatrix} , \tag{33}$$

where $\mathbf{u}_{\Omega_2}(\omega)$ is the vector of the $n_2 - n_\Gamma$ degrees of freedom related to nodes of the finite-element mesh in Ω_2 and $\mathbf{u}_\Gamma(\omega)$ is the vector of the n_Γ degrees of freedom related to the nodes on interface Γ. Consequently, the block decomposition of vector $\mathbf{f}(\omega)$ of the external forces is written as

$$\mathbf{f}(\omega) = \begin{pmatrix} \mathbf{f}_{\Omega_2}(\omega) \\ \mathbf{f}_{\Gamma}(\omega) \end{pmatrix} . \tag{34}$$

Let $\mathbf{f}^j(\omega)$ be the value of vector $\mathbf{f}(\omega)$ for which $\mathbf{f}_{\Omega_2}(\omega) = 0$ and $\{\mathbf{f}_\Gamma(\omega)\}_i = \delta_{ij}$. The boundary frequency response function $[T_\Gamma(\omega)]$ is the complex $(n_\Gamma \times n_\Gamma)$ matrix for which the components $[T_\Gamma(\omega)]_{ij}$ are such that, for each $0 < j \leq n_\Gamma$

$$[T_\Gamma(\omega)]_{ij} = \{\mathbf{u}^j_\Gamma(\omega)\}_i , \tag{35}$$

in which $\mathbf{u}^j_\Gamma(\omega)$ is the value of vector $\mathbf{u}_\Gamma(\omega)$ that is calculated in using Eq. (2) for which $\mathbf{u}_2(\omega)$ is the solution of Eq. (3) with $\mathbf{f}(\omega) = \mathbf{f}^j(\omega)$. The boundary frequency response function $[T^{\text{opt}}_\Gamma(\omega)]$ is the complex $(n_\Gamma \times n_\Gamma)$ matrix for which the components $[T^{\text{opt}}_\Gamma(\omega)]_{ij}$ are such that, for each $0 < j \leq n_\Gamma$

$$[T^{\text{opt}}_\Gamma(\omega)]_{ij} = \{\mathbf{u}^j_\Gamma(\omega)\}_i , \tag{36}$$

in which $\mathbf{u}^j_\Gamma(\omega)$ is the value of vector $\mathbf{u}_\Gamma(\omega)$ that is calculated in using Eq. (2) for which $\mathbf{u}_2(\omega)$ is the solution of Eq. (3) with $\mathbf{f}(\omega) = \mathbf{f}^j(\omega)$ and $[A_\Gamma(\omega)] = [A^{\text{opt}}_\Gamma(\omega)]$ (see Section 4) in Eq. (4). The boundary frequency response function $[T^{\text{opt}}_{\Gamma,B_k}(\omega)]$ is the complex $(n_\Gamma \times n_\Gamma)$ matrix for which the components $[T^{\text{opt}}_{\Gamma,B_k}(\omega)]_{ij}$ are such that, for each $0 < j \leq n_\Gamma$

$$[T^{\text{opt}}_{\Gamma,B_k}(\omega)]_{ij} = \{\mathbf{u}^j_{\Gamma,B_k}(\omega)\}_i , \tag{37}$$

in which $\mathbf{u}^j_{\Gamma,B_k}(\omega)$ is the value of $\mathbf{u}_{\Gamma,B_k}(\omega)$ in Eq. (14) for which $\mathbf{q}_{B_k}(\omega)$ is calculated in using the second expression in Eq. (16) where $\mathbb{u}_{2,B_k}(\omega)$ is the solution of Eq. (17) with $\mathbb{f}_{B_k}(\omega) = [P_{B_k}]^T \mathbf{f}^j(\omega)$ and $[A_{\Gamma,B_k}(\omega)] = [A^{\text{opt}}_{\Gamma,B_k}(\omega)]$ (see Section 4.5) in Eq. (19). Furthermore, distances between the three boundary frequency response functions $[T_\Gamma]$, $[T^{\text{opt}}_\Gamma]$ and $[T^{\text{opt}}_{\Gamma,B_k}]$ defined by Eq. (35) to Eq. (37) are denoted by $\varepsilon_r([T^{\text{opt}}_{\Gamma,B_k}], [T_\Gamma], B_k)$ and $\varepsilon_r([T^{\text{opt}}_\Gamma], [T_\Gamma], B_k)$ where

$$\varepsilon_r([T_1], [T_2|, B) = \frac{\sum_{\omega \in B} \|[T_1(\omega)] - [T_2(\omega)]\|_F}{\sum_{\omega \in B} \|[T_2(\omega)]\|_F} , \tag{38}$$

in which $\|[A]\|_F = \sqrt{\text{Tr}([A][A]^T)}$ is the Frobenius norm of matrix $[A]$. In addition, for given degrees of freedom numbered as i and j, we compute the following relative errors $\varepsilon_r([T^{\text{opt}}_{\Gamma,B_k}]_{ij}, [T_\Gamma]_{ij}, B_k)$ and $\varepsilon_r([T^{\text{opt}}_\Gamma]_{ij}, [T_\Gamma]_{ij}, B_k)$. These distances are related to a given frequency band B_k. A more global distance between $[T_\Gamma]$, $[T^{\text{opt}}_\Gamma]$ and $[T^{\text{opt}}_{\Gamma,B_k}]$ can be defined as

$$\varepsilon_{\text{modif}} = \max_{1 \leq k \leq n_{\text{f}}} \varepsilon_r([T^{\text{opt}}_{\Gamma,B_k}], [T_\Gamma], B_k) , \tag{39}$$

$$\varepsilon^{ij}_{\text{modif}} = \max_{1 \leq k \leq n_{\text{f}}} \varepsilon_r([T^{\text{opt}}_{\Gamma,B_k}]_{ij}, [T_\Gamma]_{ij}, B_k) , \tag{40}$$

$$\varepsilon_{\text{initial}} = \varepsilon_r([T^{\text{opt}}_\Gamma], [T_\Gamma], B_{\text{f}}) , \tag{41}$$

$$\varepsilon^{ij}_{\text{initial}} = \varepsilon_r([T^{\text{opt}}_\Gamma]_{ij}, [T_\Gamma]_{ij}, B_{\text{f}}) . \tag{42}$$

5.3 First application, a simple case

For this example, sub-domains Ω_1 and Ω_2, which model respectively a soft soil and a stiffen structure, are rectangles with dimensions 3×9 m^2 (subdomain Ω_1) and 3×3 m^2 (sub-domain Ω_2). The finite-element mesh of domain Ω_1 is constituted of 6×18 quadrangles and the finite-element mesh of Ω_2 is constituted of 6×6 quadrangles. Consequently, the number of degrees of freedom in Ω_1 is $n_1 = 452$ and the number of degree of freedom in Ω_2 is $n_2 = 184$. The total number of freedom in interface Γ is $n_\Gamma = 14$. The frequency band is $B_{\mathrm{f}} = 2\pi \times [20; 34]$ rad/s.

Table 2 shows the values of $\varepsilon_{\mathrm{modif}}$, $\varepsilon^{ij}_{\mathrm{modif}}$, $\varepsilon_{\mathrm{initial}}$ and $\varepsilon^{ij}_{\mathrm{initial}}$ for i and j equal to I or J and where the degrees of freedom $\{\mathbf{u}_2\}_I$ and $\{\mathbf{u}_2\}_J$ are respectively the displacement along the horizontal axis of a point located at the center of interface Γ and the displacement along the vertical axis of a point located at distance 0.75 meters from the center. For each computation, the number of modes per band is constant $m_k = m$ for all B_k, where m is a chosen number of modes. The number of hidden variables, which is the half of degree $d_{q,B_k} = d_q$, is also constant for all B_k. In addition, the computational duration t is given in Table 2.

A convergence analysis with respect to d_q has been carried out but it is not presented in this paper. Consequently, the value of d_q at convergence depends on m, but in this example, d_q is constant. In addition, results presented in Table 2 show that the values of $\varepsilon_{\mathrm{modif}}$ and $\varepsilon^{ij}_{\mathrm{modif}}$ tend to decrease when m increases and the computational time t increases with m. Consequently, it is possible to adjust the value of m to get a compromise between values of $\varepsilon_{\mathrm{modif}}$ or $\varepsilon^{ij}_{\mathrm{modif}}$, and the computational cost t. Such adjustment is not possible for the value of $\varepsilon_{\mathrm{initial}}$ and $\varepsilon^{ij}_{\mathrm{initial}}$ for the initial method. A reasonable value of m can be taken when $\varepsilon_{\mathrm{modif}}$ is less than 0.01. For this example, the values of $\varepsilon_{\mathrm{modif}}$ and $\varepsilon^{ij}_{\mathrm{modif}}$ with $m = 12$ for the modified method are of same order than the values of $\varepsilon_{\mathrm{initial}}$ and $\varepsilon^{ij}_{\mathrm{initial}}$ for the initial method but the computational cost is 20 times smaller. It can be noted than the modified method yields also small values of $\varepsilon_{\mathrm{modif}}$ for $m = 4$ and for which the computational cost $t = 67$ seconds which is 2900 times smaller than the computational time obtained with the initial method.

Figure 2 shows the graphs of $\|[T_\Gamma(\omega)]\|_F$, $\|[T^{\mathrm{opt}}_\Gamma(\omega)]\|_F$ and $\|[T^{\mathrm{opt}}_{\Gamma,B_k}(\omega)]\|_F$ with $m = 4$ (bottom figure), the graphs of $[T_\Gamma(\omega)]_{II}$, $[T^{\mathrm{opt}}_\Gamma(\omega)]_{II}$ and $[T^{\mathrm{opt}}_{\Gamma,B_k}(\omega)]_{II}$ with $m = 4$ (middle figure), and finally the graphs of $[T_\Gamma(\omega)]_{IJ}$, $[T^{\mathrm{opt}}_\Gamma(\omega)]_{IJ}$ and $[T^{\mathrm{opt}}_{\Gamma,B_k}(\omega)]_{IJ}$ with $m = 4$ (top figure).

It can be seen that the graphs match each other and consequently the identifications of the mass, dumping and stiffness matrices by the initial method and by the modified method are very good. In addition, it shows that a mean square estimation of the distance between $[T_\Gamma(\omega)]_{ij}$, $[T^{\mathrm{opt}}_\Gamma(\omega)]_{ij}$ and $[T^{\mathrm{opt}}_{\Gamma,B_k}(\omega)]_{ij}$ with i and j equal to I or J would be very small.

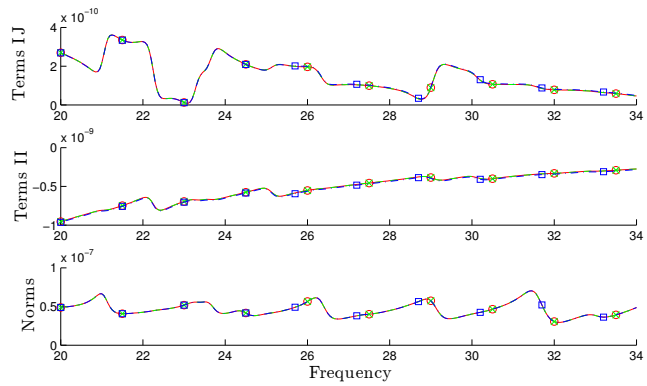

Fig. 2 Comparison between the solution of reference (finite elements method in red solid line with circular markers), the initial method (green dashed line with cross markers) and the modified method (blue dotted line with square markers) with $m = 4$. Horizontal axis: ω in Hertz. Vertical axis, on the bottom graph: $\|[T_\Gamma(\omega)]\|_F$, $\|[T^{\mathrm{opt}}_\Gamma(\omega)]\|_F$ and $\|[T^{\mathrm{opt}}_{\Gamma,B_k}(\omega)]\|_F$, on the middle graph: real parts of $[T_\Gamma(\omega)]_{II}$, $[T^{\mathrm{opt}}_\Gamma(\omega)]_{II}$ and $[T^{\mathrm{opt}}_{\Gamma,B_k}(\omega)]_{II}$ and on the top graph: real parts of $[T_\Gamma(\omega)]_{IJ}$, $[T^{\mathrm{opt}}_\Gamma(\omega)]_{IJ}$ and $[T^{\mathrm{opt}}_{\Gamma,B_k}(\omega)]_{IJ}$.

Moreover, for this first example, the use of several frequency bands B_k ($n_{\mathrm{f}} > 1$) does not bring any advantage with respect to the initial method. Nevertheless, the reduction of the displacement at the interface (Section 3.3) allows to decrease the computational cost by a factor 20.

5.4 Second application, case with an extended frequency band B_{f}

In the second example, sub-domains Ω_1 and Ω_2, which model respectively a soft soil and a stiffen structure, are rectangles with dimensions 3×9 m^2 (sub-domain Ω_1) and 3×3 m^2 (sub-domain Ω_2). The finite-element mesh of domain Ω_1 is constituted of 6×18 quadrangles and the finite-element mesh of Ω_2 is constituted of 6×6 quadrangles. Consequently, the number of degrees of freedom in Ω_1 is $n_1 = 452$ and the number of degree of freedom in Ω_2 is $n_2 = 184$. The total number of freedom in interface Γ is $n_\Gamma = 14$. The frequency band is $B_{\mathrm{f}} = 2\pi \times [20; 100]$ rad/s.

Table 3 shows the values of $\varepsilon_{\text{modif}}$, $\varepsilon^{ij}_{\text{modif}}$, $\varepsilon_{\text{initial}}$ and $\varepsilon^{ij}_{\text{initial}}$ for i and j equal to I or J and where the degrees of freedom $\{\mathbf{u}_2\}_I$ and $\{\mathbf{u}_2\}_J$ are respectively the displacement along the horizontal axis of a point located at the center of interface Γ and the displacement along the vertical axis of a point located at distance 0.75 meters from the center. For each computations, the number of modes per band is constant $m_k = m$ for all B_k. The number of hidden variables, which is the half of degree $d_{q,B_k} = d_q$, is also constant for all B_k. In addition, the computational duration t is given in Table 3.

As in the first example, a convergence analysis with respect to d_q has been carried out but it is not presented in this paper. Consequently, the value of d_q at convergence depends on m, but in this example, d_q is constant. In addition, results presented in Table 3 show that the values of $\varepsilon_{\text{modif}}$ and $\varepsilon^{ij}_{\text{modif}}$ tend to decrease when m increases and the computational time t increases with m. For this example, the values of $\varepsilon_{\text{modif}}$ and $\varepsilon^{ij}_{\text{modif}}$ with $m = 12$ for the modified method are of same order than the values of $\varepsilon_{\text{initial}}$ and $\varepsilon^{ij}_{\text{initial}}$ for the initial method but the computational cost is 10 times smaller. It can be noted than the modified method yields also small values of $\varepsilon_{\text{modif}}$ for $m = 6$ and for which the computational cost $t = 3688$ seconds which is 345 times smaller than the computational time obtained with the initial method.

Figure 3 shows the graphs of $\|[T_\Gamma(\omega)]\|_F$, $\|[T^{\text{opt}}_\Gamma(\omega)]\|_F$ and $\|[T^{\text{opt}}_{\Gamma,B_k}(\omega)]\|_F$ with $m = 6$ (bottom figure), the graphs of $[T_\Gamma(\omega)]_{II}$, $[T^{\text{opt}}_\Gamma(\omega)]_{II}$ and $[T^{\text{opt}}_{\Gamma,B_k}(\omega)]_{II}$ with $m = 6$ (middle figure) and finally the graphs of $[T_\Gamma(\omega)]_{IJ}$, $[T^{\text{opt}}_\Gamma(\omega)]_{IJ}$ and $[T^{\text{opt}}_{\Gamma,B_k}(\omega)]_{IJ}$ with $m = 6$ (top figure). It can be seen that the graphs match each other and consequently the identifications of the mass, dumping and stiffness matrices by the initial method and by the modified method are very good. In addition, it shows that a mean square estimation of the distance between $[T_\Gamma(\omega)]_{ij}$, $[T^{\text{opt}}_\Gamma(\omega)]_{ij}$ and $[T^{\text{opt}}_{\Gamma,B_k}(\omega)]_{ij}$ with i and j equal to I or J would be very small. It can be noted that continuity between frequency bands B_k is apparently respected.

In this case, the decomposition of frequency band B_{f} and the interface reduction allow a reduction of the computational cost by a factor 10. In addition, for an equivalent accuracy the initial method doesn't yields causal model of boundary dynamic stiffness matrices. And consequently, the identified mass, damping and stiffness matrices can not be used for constructing a probabilistic model of random boundary dynamic stiffness matrices.

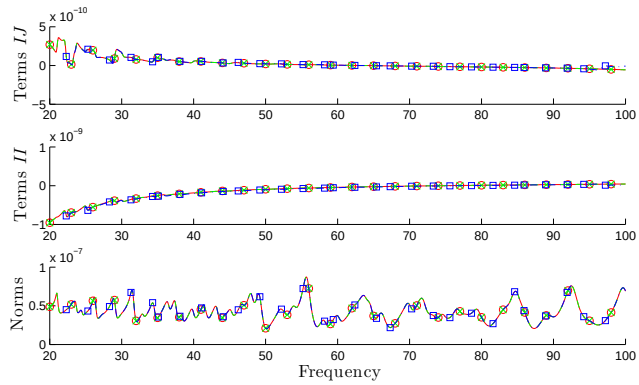

Fig. 3 Comparison between the solution of reference (finite elements method in red solid line with circular markers), the initial method (green dashed line with cross markers) and the modified method (blue dotted line with square markers) with $m = 6$. Horizontal axis: ω in Hertz. Vertical axis, on the bottom graph: $\|[T_\Gamma(\omega)]\|_F$, $\|[T^{\text{opt}}_\Gamma(\omega)]\|_F$ and $\|[T^{\text{opt}}_{\Gamma,B_k}(\omega)]\|_F$, on the middle graph: real parts of $[T_\Gamma(\omega)]_{II}$, $[T^{\text{opt}}_\Gamma(\omega)]_{II}$ and $[T^{\text{opt}}_{\Gamma,B_k}(\omega)]_{II}$ and on the top graph: real parts of $[T_\Gamma(\omega)]_{IJ}$, $[T^{\text{opt}}_\Gamma(\omega)]_{IJ}$ and $[T^{\text{opt}}_{\Gamma,B_k}(\omega)]_{IJ}$.

5.5 Third application, case with an extended interface Γ

In this third example, sub-domains Ω_1 and Ω_2, which model respectively a soft soil and a stiffen structure, are rectangles with dimensions 6×18 m^2 (sub-domain Ω_1) and 6×6 m^2 (sub-domain Ω_2). The finite-element mesh of domain Ω_1 is constituted of 12×36 quadrangles and the finite-element mesh of Ω_2 is constituted of 12×12 quadrangles. Consequently, the number of degrees of freedom in Ω_1 is $n_1 = 902$ and the number of degree of freedom in Ω_2 is $n_2 = 366$. The total number of freedom in interface Γ is $n_\Gamma = 26$. The frequency band is $B_{\text{f}} = 2\pi \times [20; 34]$ rad/s.

Table 4 shows the values of $\varepsilon_{\text{modif}}$ and $\varepsilon^{ij}_{\text{modif}}$ for i and j equal to I or J and where the degrees of freedom $\{\mathbf{u}_2\}_I$ and $\{\mathbf{u}_2\}_J$ are respectively the displacement along the horizontal axis of a point located at the center of interface Γ and the displacement along the vertical axis of a point located at distance 1.5 meters from the center. For each computations, the number of modes per band is constant $m_k = m$ for all B_k, with m a chosen number of modes. The number of hidden variables, which is the half of degree $d_{q,B_k} = d_q$, is also constant for all B_k. In addition, the computational duration t is given in Table 4.

Results presented in Table 4 show that the values of $\varepsilon_{\text{modif}}$ and $\varepsilon^{ij}_{\text{modif}}$ tend to decrease when m increases and the computational time t increases with m. Nevertheless, for $m = 1$ and $m = 2$, the modal density

leads to very small frequency bands B_k. The number of available frequency points inside such bands B_k is then less that needed for applying the hidden state variables method. This explains numbers of band n_f which are lower or equal than the n_f indicated for $m = 3$. It can be noted than the modified method yields also small values of $\varepsilon_{\text{modif}}$ for $m = 4$ and for which the computational cost is $t = 736$ seconds.

Figure 4 shows graphs of $\|[T_\Gamma(\omega)]\|_F$ and $\|[T^{\text{opt}}_{\Gamma,B_k}(\omega)]\|_F$ with $m = 8$ (bottom figure), the graphs of $[T_\Gamma(\omega)]_{II}$ and $[T^{\text{opt}}_{\Gamma,B_k}(\omega)]_{II}$ with $m = 8$ (middle figure) and the graphs of $[T_\Gamma(\omega)]_{IJ}$ and $[T^{\text{opt}}_{\Gamma,B_k}(\omega)]_{IJ}$ with $m = 8$ (top figure). It can be seen that the graphs match each other and consequently the identification of the mass, dumping and stiffness matrices by the modified method is good. In addition, it shows that a mean square estimation of the distance between $[T_\Gamma(\omega)]_{ij}$ and $[T^{\text{opt}}_{\Gamma,B_k}(\omega)]_{ij}$ with i and j equal to I or J would be small. The identified values in the middle of Figure 4 are moved from the references values but have similar behaviour than the solution of reference.

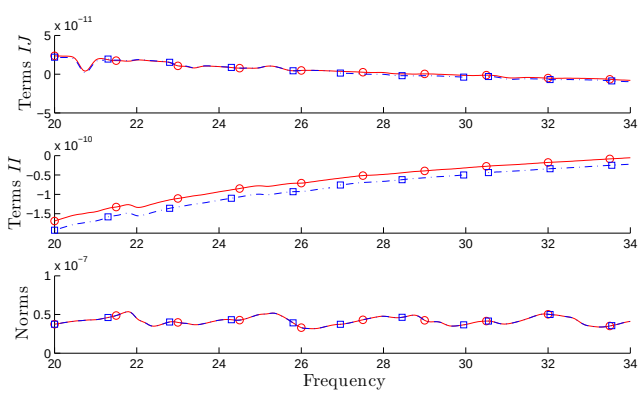

Fig. 4 Comparison between the solution of reference (finite elements method in red solid line with circular markers) and the modified method (blue dotted line with square markers) with $m = 8$. Horizontal axis: ω in Hertz. Vertical axis, on the bottom graph: $\|[T_\Gamma(\omega)]\|_F$ and $\|[T^{\text{opt}}_{\Gamma,B_k}(\omega)]\|_F$, on the middle graph: real parts of $[T_\Gamma(\omega)]_{II}$ and $[T^{\text{opt}}_{\Gamma,B_k}(\omega)]_{II}$ and on the top graph: real parts of $[T_\Gamma(\omega)]_{IJ}$ and $[T^{\text{opt}}_{\Gamma,B_k}(\omega)]_{IJ}$.

In this case, initial method is not able to identify the mass, damping and stiffness matrices because of a computational cost that is too much important and it is not worth it. Nevertheless, the modified method is able to identify the mass, damping and stiffness matrices which yields a causal model of boundary dynamic stiffness matrices.

5.6 Fourth application, case with an extended interface Γ and an extended frequency band B_{f}

In this last example, sub-domains Ω_1 and Ω_2, which model respectively a soft soil and a stiffen structure, are rectangles with dimensions 6×18 m^2 (sub-domain Ω_1) and 6×6 m^2 (sub-domain Ω_2). The finite-element mesh of domain Ω_1 is constituted of 12×36 quadrangles and the finite-element mesh of Ω_2 is constituted of 12×12 quadrangles. Consequently, the number of degrees of freedom in Ω_1 is $n_1 = 902$ and the number of degree of freedom in Ω_2 is $n_2 = 366$. The total number of freedom in interface Γ is $n_\Gamma = 26$. The frequency band is $B_{\text{f}} = 2\pi \times [10; 45]$ rad/s.

Table 5 shows the values of $\varepsilon_{\text{modif}}$ and $\varepsilon^{ij}_{\text{modif}}$ for i and j equal to I or J and where the degrees of freedom $\{\mathbf{u}_2\}_I$ and $\{\mathbf{u}_2\}_J$ are respectively the displacement along the horizontal axis of a point located at the center of interface Γ and the displacement along the vertical axis of a point located at distance 1.5 meters from the center. For each computations, the number of modes per band is constant $m_k = m$ for all B_k. The number of hidden variables, which is the half of degree $d_{q,B_k} = d_q$, is also constant for all B_k. In addition, the computational duration t is given in Table 5.

Results presented in Table 5 show that the values of $\varepsilon_{\text{modif}}$ and $\varepsilon^{ij}_{\text{modif}}$ tend to decrease when m increases and the computational time t increases with m. Consequently, a compromise between values of $\varepsilon_{\text{modif}}$ or $\varepsilon^{ij}_{\text{modif}}$, and the computational cost t is possible. As previously, for $m = 1$ and $m = 2$ the frequency bands B_k can be very small. In such cases, the density of frequencies has to be high. It can be noted than the modified method yields also small values of $\varepsilon_{\text{modif}}$ for $m = 6$ and for which the computational cost is $t = 8325$ seconds.

Figure 5 shows graphs of $\|[T_\Gamma(\omega)]\|_F$ and $\|[T^{\text{opt}}_{\Gamma,B_k}(\omega)]\|_F$ with $m = 8$ (bottom figure), the graphs of $[T_\Gamma(\omega)]_{II}$ and $[T^{\text{opt}}_{\Gamma,B_k}(\omega)]_{II}$ with $m = 8$ (middle figure) and the graphs of $[T_\Gamma(\omega)]_{IJ}$ and $[T^{\text{opt}}_{\Gamma,B_k}(\omega)]_{IJ}$ with $m = 8$ (top figure). It can be seen that the graphs match each other and consequently the identification of the mass, dumping and stiffness matrices by the modified method is good. In addition, it shows that a mean square estimation of the distance between $[T_\Gamma(\omega)]_{ij}$ and $[T^{\text{opt}}_{\Gamma,B_k}(\omega)]_{ij}$ with i and j equal to I or J would be small.

In this case, initial method is not able to identify the mass, damping and stiffness matrices because of a computational cost that is too much important and it is not worth it. Nevertheless, the modified method is able to identify the mass, damping and stiffness matri-

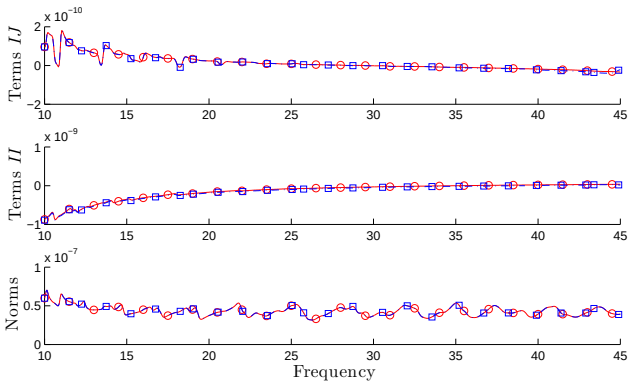

Fig. 5 Comparison between the solution of reference (finite elements method in red solid line with circular markers) and the modified method (blue dotted line with square markers) with $m = 8$. Horizontal axis: ω in Hertz. Vertical axis, on the bottom graph: $\|[T_\Gamma(\omega)]\|_F$ and $\|[T^{\rm opt}_{\Gamma,B_k}(\omega)]\|_F$, on the middle graph: real parts of $[T_\Gamma(\omega)]_{II}$ and $[T^{\rm opt}_{\Gamma,B_k}(\omega)]_{II}$ and on the top graph: real parts of $[T_\Gamma(\omega)]_{IJ}$ and $[T^{\rm opt}_{\Gamma,B_k}(\omega)]_{IJ}$.

ces which yields a causal model of boundary dynamic stiffness matrices.

6 Probabilistic model of boundary dynamic stiffness matrix

6.1 Random boundary dynamic stiffness matrix

For each frequency band B_k, we define the random stiffness matrix $[\mathbf{A}_{1,B_k}(\omega)]$ as

$$[\mathbf{A}_{1,B_k}(\omega)] = -\omega^2[\mathbf{M}_{1,B_k}] + \jmath\,\omega[\mathbf{D}_{1,B_k}] + [\mathbf{K}_{1,B_k}] \ , \quad (43)$$

where random matrices $[\mathbf{M}_{1,B_k}]$, $[\mathbf{D}_{1,B_k}]$ and $[\mathbf{K}_{1,B_k}]$ belong to the stochastic set of random matrices SE^+ introduced by C. Soize in [14,13]. Introducing those random matrices allows the uncertainties related to the modelling of matrices $[M^{\rm opt}_{1,B_k}]$, $[D^{\rm opt}_{1,B_k}]$ and $[K^{\rm opt}_{1,B_k}]$ to be taken into account. Their probabilistic models depend on three dispersion parameters δ_{M,B_k}, δ_{D,B_k}, δ_{K,B_k} which control the level of uncertainties related to $[M^{\rm opt}_{1,B_k}]$, $[D^{\rm opt}_{1,B_k}]$, and $[K^{\rm opt}_{1,B_k}]$. In addition random matrices $[\mathbf{M}_{1,B_k}]$, $[\mathbf{D}_{1,B_k}]$, and $[\mathbf{K}_{1,B_k}]$ are written as

$$[\mathbf{M}_{1,B_k}] = [L^{\rm opt}_{M,B_k}]\,[\mathbf{G}_{M,B_k}]\,[L^{\rm opt}_{M,B_k}]^T \ , \quad (44)$$

$$[\mathbf{D}_{1,B_k}] = [L^{\rm opt}_{D,B_k}]\,[\mathbf{G}_{D,B_k}]\,[L^{\rm opt}_{D,B_k}]^T \ , \quad (45)$$

$$[\mathbf{K}_{1,B_k}] = [L^{\rm opt}_{K,B_k}]\,[\mathbf{G}_{K,B_k}]\,[L^{\rm opt}_{K,B_k}]^T \ , \quad (46)$$

in which matrices $[M_{1,B_k}] = [L^{\rm opt}_{M,B_k}]\,[L^{\rm opt}_{M,B_k}]^T$, $[D_{1,B_k}] = [L^{\rm opt}_{D,B_k}]\,[L^{\rm opt}_{D,B_k}]^T$, and $[K_{1,B_k}] = [L^{\rm opt}_{K,B_k}]\,[L^{\rm opt}_{K,B_k}]^T$ are the Cholesky factorizations of matrices $[M^{\rm opt}_{1,B_k}]$, $[D^{\rm opt}_{1,B_k}]$, and $[K^{\rm opt}_{1,B_k}]$ and in which the random real $(m_k \times m_k)$ matrices $[\mathbf{G}_{M,B_k}]$, $[\mathbf{G}_{D,B_k}]$, and $[\mathbf{G}_{K,B_k}]$ belong to the set SG^+ introduced by C. Soize in [14,13]. A probabilistic model of uncertainties related to the boundary dynamic stiffness matrices $[A_\Gamma(\omega)]$ is then constructed for each frequency band B_k in substituting the deterministic matrix $[A_{B_k}(\omega)]$ in Eq. (17) by a random matrix $[\mathbf{A}_{B_k}(\omega)]$ and in substituting the deterministic vector $\mathbb{u}_{2,B_k}(\omega)$ by a random vector $\mathbb{U}_{2,B_k}(\omega)$ such that

$$([A_{2,B_k}(\omega)] + [\mathbf{A}_{B_k}(\omega)])\,\mathbb{U}_{2,B_k}(\omega) = \mathbb{f}_{B_k}(\omega) \ , \quad (47)$$

The random matrix $[\mathbf{A}_{B_k}(\omega)]$ is written as

$$[\mathbf{A}_{B_k}(\omega)] = \begin{pmatrix} [0_2] & \\ & [\mathbf{A}_{\Gamma,B_k}(\omega)] \end{pmatrix} \ , \quad (48)$$

in which $[\mathbf{A}_{\Gamma,B_k}(\omega)]$ is a random symmetric $(m^+_{B_k} \times m^+_{B_k})$ matrix such that

$$[\mathbf{A}_{\Gamma,B_k}(\omega) = [\mathbf{A}_{1\Gamma,B_k}(\omega)] - [\mathbf{A}_{1c,B_k}(\omega)]\,[\mathbf{A}_{1h,B_k}(\omega)]^{-1}[\mathbf{A}_{1c,B_k}(\omega)]^T \ , \quad (49)$$

where random complex matrices $[\mathbf{A}_{1\Gamma,B_k}(\omega)]$, $[\mathbf{A}_{1c,B_k}(\omega)]$, $[\mathbf{A}_{1h,B_k}(\omega)]$ and $[\mathbf{A}_{1c,B_k}(\omega)]$ are extracted from the following block decomposition of random matrix $[\mathbf{A}_{1,B_k}(\omega)]$

$$[\mathbf{A}_{1,B_k}(\omega)] = \begin{pmatrix} [\mathbf{A}_{1h,B_k}(\omega)] & [\mathbf{A}_{1c,B_k}(\omega)] \\ [\mathbf{A}_{1c,B_k}(\omega)]^T & [\mathbf{A}_{1\Gamma,B_k}(\omega)] \end{pmatrix} \ . \quad (50)$$

Consequently, for each frequency band B_k, the finite element vector of the degree of freedom in domain Ω_2 is modelled by a random vector $\mathbf{U}_{2,B_k}(\omega)$ which is constructed in substituting $\mathbb{u}_{2,B_k}(\omega)$ by $\mathbb{U}_{2,B_k}(\omega)$ in Eq. (15). We then have

$$\mathbf{U}_{2,B_k}(\omega) = [P_{B_k}]\,\mathbb{U}_{2,B_k}(\omega) \ . \quad (51)$$

It should be noted that without any additional information concerning the statistics between $[\mathbf{A}_{\Gamma,B_k}(\omega)]$ and $[\mathbf{A}_{\Gamma,B_\ell}(\omega)]$ with $\ell \neq k$ then, for all ℓ and k, matrices $[\mathbf{G}_{M,B_k}]$, $[\mathbf{G}_{M,B_\ell}]$, $[\mathbf{G}_{D,B_k}]$, $[\mathbf{G}_{D,B_\ell}]$, $[\mathbf{G}_{K,B_k}]$, and, $[\mathbf{G}_{K,B_\ell}]$ are six statistical independent random matrices for all ℓ and k.

6.2 Example of random boundary frequency response function

For same case as in section 5.3, we compute 200 stochastic realizations of random boundary dynamic stiffness matrix $[\mathbf{A}_{\Gamma,B_k}(\omega)]$. It allows to construct 200 random boundary frequency response matrices $[\mathbf{T}_{\Gamma,B_k}(\omega)]$ by Eq. (37) where the displacement interpolation is obtained by Eq. (51). The number of modes per band m is chosen as $m = 6$ and dispersion parameters are equal, $\delta_{M,B_k} = \delta_{D,B_k} = \delta_{K,B_k} = 0.3$ for both frequency bands

B_k ($n_f = 2$).
Figure 6 shows three parts, relative to the norm of the boundary frequency response matrix $\|[\mathbf{T}^{\text{opt}}_{\Gamma,B_k}(\omega)]\|_F$, and the two components $[\mathbf{T}^{\text{opt}}_{\Gamma,B_k}(\omega)]_{II}$ and $[\mathbf{T}^{\text{opt}}_{\Gamma,B_k}(\omega)]_{IJ}$. On the three parts, the values of reference $\|[T_\Gamma(\omega)]\|_F$, $[T_\Gamma(\omega$ and $[T_\Gamma(\omega)]_{IJ}$ are plotted in red lines. One stochastic realization of $\|[\mathbf{T}^{\text{opt}}_{\Gamma,B_k}(\omega)]\|_F$, $[\mathbf{T}^{\text{opt}}_{\Gamma,B_k}(\omega)]_{II}$ and $[\mathbf{T}^{\text{opt}}_{\Gamma,B_k}(\omega)$ are also presented in dashed black line. In addition, deterministic values $\|[T^{\text{opt}}_{\Gamma,B_k}(\omega)]\|_F$, $[T^{\text{opt}}_{\Gamma,B_k}(\omega)]_{II}$ and $[T^{\text{opt}}_{\Gamma,B_k}$ are plotted in dashed blue lines. The 90% confidence intervals computed with 200 realizations are shown in green solid line. With Figure 6, it can be noted that constant δ parameters on B_{f} seems allow the keeping of the continuity on each stochastic realizations (near 29Hz). Because of the large values of δ_{M,B_k}, δ_{D,B_k} and δ_{K,B_k}, the dispersion indicated by the 90% confidence interval is large compared with the variation of deterministic values. The dispersion in Forbenius norm is less accented, but respects the aspect of the dispersions of components.

The new stochastic model exposed in this numerical example is not similar to the initial model. The cross-correlation between the different frequency bands have no meaning. In state, the stochastic model allows to choose different deviation parameters for each groups of eigen modes. This can be interpreted by a variation of the own dimensions of the structure. It allows to measure the impact of variations of the eigen modes of the structure on its dynamical behaviour.

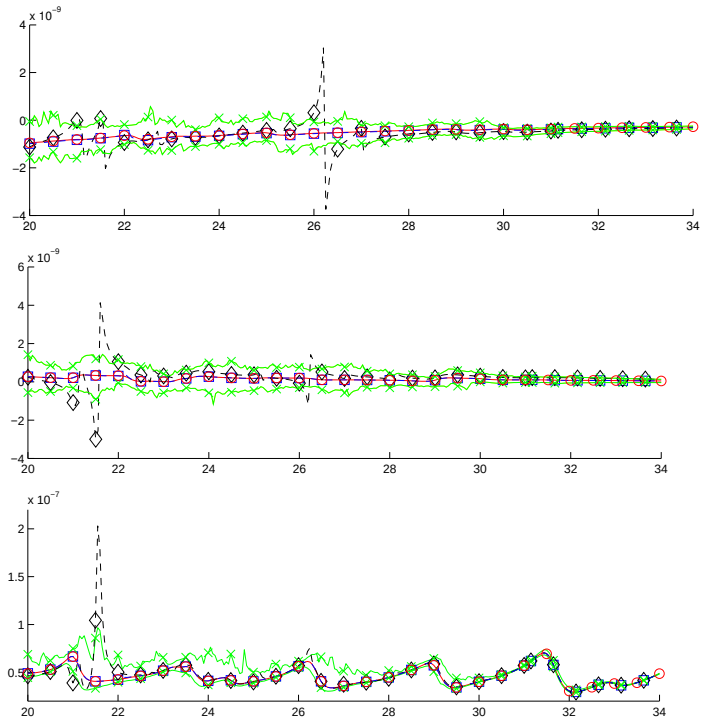

Fig. 6 Statistical results; Horizontal axis: ω in Hertz. Vertical axis, on bottom graph norms of: matrix of reference (red solid line with circular markers) $\|[T_\Gamma(\omega)]\|_F$, deterministic reduced matrix (blue dotted line with square markers) $\|[T^{\text{opt}}_{\Gamma,B_k}(\omega)]\|_F$, a random realization of $\|[\mathbf{T}^{\text{opt}}_{\Gamma,B_k}(\omega)]\|_F$ (black dashed line with diamond markers) and 90% confidence interval (green solid lines with cross markers), on middle graph the II components of: $[T_\Gamma(\omega)]$ (red solid line with circular markers), $[T^{\text{opt}}_{\Gamma,B_k}(\omega)]$ (blue dotted line with square markers), $\|[\mathbf{T}^{\text{opt}}_{\Gamma,B_k}(\omega)]\|_F$ (black dashed line with diamond markers) and 90% confidence interval (green sold line with cross markers), on top graph the IJ components of: $[T_\Gamma(\omega)]$ (red solid line with circular markers), $[T^{\text{opt}}_{\Gamma,B_k}(\omega)]$ (blue dotted line with square markers), $[\mathbf{T}^{\text{opt}}_{\Gamma,B_k}(\omega)]|_F$ (black dashed line with diamond markers) and 90% confidence interval (green sold line with cross markers).

7 Conclusion

We present a reduction method of the hidden state variables method which is subdivided on smallest frequency bands with restrained number of modes. The polynomial bases, used in the identification process, are now dimensioned by the number of modes chosen for each sub-problems. Besides the fact that each sub-problem can be treated in parallel, substantial gain of the computational time is possible. For a equivalent precision the computational cost is 10 to 20 times less than in the initial method. For an acceptable precision, the computational cost could be more than 1000 times smaller. Then, we show that the loss of precision is acceptable in terms of spared time. In addition, when size of the boundary dynamical stiffness matrix grows up, the precision stay good with enough modes. In such cases initial method is not able to identify the mass, damping and stiffness matrices because of a computational cost that is too much important.

Nevertheless, the approach needs several eigen modes and a sufficient density of frequencies in respect to the density of modes. However, further study should be done to obtain equivalent statistical characteristics as the initial method.

References

1. O. C. Zienkiewicz, R. L. Taylor and J. Z. Zhu (2005) The finite element method, volume 1. Butterworth-Heinemann, sixth edition.
2. D. Givoli (1992) Numerical Methods for Problems in Infinite Domains. Studies in Applied Mechanics. Elsevier.
3. J. P. Wolf and C. Song (1996) Finite-element modelling of unbounded media. Wiley, Chichester.
4. E. Turkel (1998) Special issue on absorbing boundary conditions. Applied Numerical Mathematics, 27(4):327–560.
5. F. Magoulès and I. Harari (2006) Absorbing boundary conditions. Computer Methods in Applied Mechanics and Engineering, 195(29-32):3551–3902.

6. S. V. Tsynkov (1998) Numerical solution of problems on unbounded domains. a review. Applied Numerical Mathematics, 27:465–532.
7. M. Bonnet (1999) Boundary Integral Equation Methods for Solids and Fluids. Wiley-Blackwell.
8. J. P. Wolf and C. Song (2001) The scaled boundary finite-element method - a fundamental solution-less boundary-element method. Computer Methods in Applied Mechanics and Engineering, 190(42):5551–5568.
9. J. Mondot, B. Petersson (1987) Characterization of strutureborne sound sources: The source descriptor and the coupling function. Journal of sound and vibration 114:507–518.
10. Y. Koh, R. White (1996) Analysis and control of vibration power transmission to machinery supporting structures subjected to a multi-excitation system, Part I: Driving point mobility matrix of beams and rectangular plates. Journal of sound and vibration 196:469–493.
11. M. Villot, P. Ropars, E. Bongini, et al (2011) Modelling the influence of structural modifications on the response of a building to railway vibration. Noise control Engineering Journal 59:641–651.
12. A. Cherukuri, P. E. Barbone (1998) High modal density approximation for equipment in the time domain. Journal of Acoustical Society of America 104(2):2048–2053.
13. C. Soize (2000) A nonparametric model of random uncertainties for reduced matrix models in structural dynamics. Probabilistic engineering mechanics 15:277–294.
14. C. Soize (2005) Random matrix theory for modeling uncertainties in computational mechanics. Computer methods in applied mechanics and engineering 194:1333–1366.
15. R. Cottereau, D. Clouteau, C. Soize (2007) Construction of a probabilistic model for impedance matrices. Comput. Methods Appl. Mech. Engrg. 196:2252–2268.
16. R. Cottereau, D. Clouteau, C. Soize (2006) Probabilistic nonparametric model of impedance matrices: Application to the seismic design of a structure. European Journal of Computational Mechanics 15:131–142.
17. P. Ropars, C. Desceliers, P. Jean (2014) Quantification of uncertainties in a computational model of interaction soil-structure with a railway excitation. submit on October 2014 in Journal of Vibration and Acoustics.
18. F. Chabas, C. Soize (1987) Modeling mechanical subsystems by boundary impedance in the finite element method. La Recherche Aérospatiale (english edition), 5:59–75.
19. P. Ropars, G. Bonnet, P. Jean (2014) A stabilization process applied to a hidden variables method for evaluating the uncertainties on foundation impedances and their effect on vibrations induced by railways in a building. Journal of Sound and Vibration 333(1):1953–1971.
20. J. W. S. Rayleigh (1945) The theory of sound. Volume 1, Diver Publications, New York.
21. A. Dienstfrey, L. Greengard (2001) Analytic continuation, singular-value expansions, and Kramers-Kronig analysis. Inverse Problems 17:1307–1320.
22. R. Cottereau, D. Clouteau, C. Soize (2007) Modèle dynamique équivalent de matrices d'impédance de fondation. 7ème Colloque National, AFPS 2007 - École Centrale Paris.
23. M. I. Friswell (1990) Candidate reduced order models for structural parameter estimation. Journal of Vibration and Acoustics 112:93–97.
24. R. R. Craig (1995) Substructure methods in vibration. Journal of Vibration and Acoustics 117(3):207–203.
25. S. Chaillat and M. Bonnet (2014) A new Fast Multipole formulation for the elastodynamic half-space Green's tensor. Journal of Computational Physics, 258:787–808.
26. M. H. Bazyar and C. Song (2008) A continued-fraction-based high-order transmitting boundary for wave propagation in unbounded domains of arbitrary geometry. International Journal for Numerical Methods in Engineering 74:209–237.
27. S. Tang, T. Y. Hou and W. K. Liu (2006) A mathematical framework of the bridging scale method. International Journal for Numerical Methods in Engineering 65:1688–1713.
28. P. E. Barbone, A. Cherukuri, D. Goldman (2000) Canonical representation of complex vibratory subsystems: time domain Dirichlet to Neumann maps. International Journal of Solids and Structures 37:2825–2857.
29. P. E. Barbone, D. Givoli, I. Patlashenko (2003) Optimal modal reduction of vibrating substructures. International Journal for Numerical Methods in Engineering 57:341–369.
30. D. Givoli, P. E. Barbone, I. Patlashenko (2004) Which are the important modes of a subsystem? International Journal for Numerical Methods in Engineering, 59:1657–1678.
31. C. Sanathanan, J. Koerner (1963) Transfer function synthesis as a ratio of two complex polynomials. IEEE Transaction on Automatic Control 56–58.
32. X. Du, M. Zhao (2009) Stability and identification for rational approximation of frequency response function of unbounded soil. Earthquake Engineering and Structural Dynamic 39:165–186.

Table 2 Convergence analysis with respect to the number of modes per band m

m	n_f	d_q	$\varepsilon_{\text{modif}}$	$\varepsilon^{I\,I}_{\text{modif}}$	$\varepsilon^{J\,J}_{\text{modif}}$	$\varepsilon^{I\,J}_{\text{modif}}$	$t\ (s)$
1	7	4	0,4667	0,9893	0,8490	0,9868	27
2	4	4	0,1025	0,9957	0,9832	0,9926	37
3	3	4	0,0248	0,4244	0,9767	2,0145	55
4	2	4	0,0003206	0,0454	0,0160	0,0088	67
6	2	4	0,0001670	0,0412	0,0051	0,0176	255
8	1	4	0,00000895	0,0213	0,0015	0,0010	954
10	1	4	0,00000608	0,0261	0,0009	0,0127	2759
12	1	4	0,00000296	0,0028	0,0004	0,0047	9747
n_Γ	n_f	d_q	$\varepsilon_{\text{intial}}$	$\varepsilon^{I\,I}_{\text{initial}}$	$\varepsilon^{J\,J}_{\text{initial}}$	$\varepsilon^{I\,J}_{\text{initial}}$	$t\ (s)$
14	1	4	0,000000509	0,0000677	0,0003452	0,0008712	194234

Table 3 Convergence study of the reduced method in respect to number of modes per band m

m	n_f	d_q	$\varepsilon_{\text{modif}}$	$\varepsilon^{I\,I}_{\text{modif}}$	$\varepsilon^{J\,J}_{\text{modif}}$	$\varepsilon^{I\,J}_{\text{modif}}$	$t\ (s)$
1	42	4	0,5693	162,9618	10,3921	206,3245	154
2	30	4	0,1813	11,4529	8,1665	32,5976	321
3	21	4	0,0445	4,8319	10,2162	38,6399	852
4	16	4	0,0135	8,7591	2,5721	30,5562	1016
6	11	4	0,0055	1,0313	1,1461	1,4587	3688
8	8	4	0,000475	0,6813	0,2395	0,2296	12367
10	8	4	0,000218	0,5239	0,2114	0,2037	40863
12	6	4	0,0000386	0,1584	0,0147	0,0244	130725
n_Γ	n_f	d_q	$\varepsilon_{\text{intial}}$	$\varepsilon^{I\,I}_{\text{initial}}$	$\varepsilon^{J\,J}_{\text{initial}}$	$\varepsilon^{I\,J}_{\text{initial}}$	$t\ (s)$
14	1	8	0,0000084588	0,0011	0,0002	0,0011	1272042

Table 4 Convergence study of the reduced method in respect to number of modes per band m

m	n_f	d_q	$\varepsilon_{\text{modif}}$	$\varepsilon^{I\,I}_{\text{modif}}$	$\varepsilon^{J\,J}_{\text{modif}}$	$\varepsilon^{I\,J}_{\text{modif}}$	$t\ (s)$
1	8	4	0,2638	13,2821	0,9994	42,4894	106
2	9	4	1,2161	1,6721	11,9184	82,8458	199
3	9	4	0,1125	5,2505	1,9853	11,2665	617
4	7	4	0,0014	2,5034	0,8715	21,3065	736
6	5	4	0,0004933	1,5117	0,1491	3,0762	3765
8	4	4	0,0002532	1,0135	0,0853	1,2228	9310
10	3	4	0,0001112	0,8393	0,0705	0,2563	27709
12	3	4	0,0000533	0,7776	0,0368	0,1006	132549

Table 5 Convergence study of the reduced method in respect to number of modes per band m

m	n_f	d_q	$\varepsilon_{\text{modif}}$	$\varepsilon^{I\,I}_{\text{modif}}$	$\varepsilon^{J\,J}_{\text{modif}}$	$\varepsilon^{I\,J}_{\text{modif}}$	$t\ (s)$
1	14	4	1,6641	114,1307	5,7465	875,0511	198
2	21	4	1,4433	144,4693	7,3431	49,5112	387
3	22	4	0,9317	57,1797	7,0027	47,8213	1251
4	17	4	0,2688	12,3305	3,2065	20,3804	1522
6	12	4	0,0048	7,6171	0,9880	4,5339	8325
8	9	4	0,0028	1,6416	0,9888	1,3611	22552
10	8	4	0,00080232	1,0051	0,1582	0,2669	69114
12	7	4	0,00026208	1,1289	0,1391	0,0952	415586